Syntheses of dibenzo[*d,d'*]benzo[2,1-*b*:3,4-*b'*]difuran derivatives and their application to organic field-effect transistors

Minh Anh Truong and Koji Nakano[*]

Address:
Department of Organic and Polymer Materials Chemistry, Tokyo University of Agriculture and Technology, 2-24-16 Naka-cho, Koganei, Tokyo 184-8588, Japan

Email:
Koji Nakano[*] - k_nakano@cc.tuat.ac.jp

* Corresponding author

Abstract

Ladder-type π-conjugated compounds containing a benzo[2,1-*b*:3,4-*b'*]difuran skeleton, such as dibenzo[*d,d'*]benzo[2,1-*b*:3,4-*b'*]difuran (*syn*-DBBDF) and dinaphtho[2,3-*d*:2',3'-*d'*]benzo[2,1-*b*:3,4-*b'*]difuran (*syn*-DNBDF) were synthesized. Their photophysical and electrochemical properties were revealed by UV–vis absorption and photoluminescence spectroscopy and cyclic voltammetry. Organic field-effect transistors (OFETs) were fabricated with these compounds as organic semiconductors, and their semiconducting properties were evaluated. OFETs with *syn*-DBBDF and *syn*-DNBDF showed typical p-type characteristics with hole mobilities of $<1.5 \times 10^{-3}$ $cm^2 \cdot V^{-1} \cdot s^{-1}$ and $<1.0 \times 10^{-1}$ $cm^2 \cdot V^{-1} \cdot s^{-1}$, respectively.

Introduction

Organic semiconductors have significantly been developed in the past two decades by virtue of their advantages, such as low weight, flexibility, large-area processability, which are different features from conventional silicon-based semiconductors. Organic semiconducting materials can be used as active layers in organic field-effect transistors (OFETs) [1-7], organic light-emitting diodes (OLEDs) [8-10], and organic photovoltaics (OPVs) [11,12]. Among many organic semiconducting materials so far reported, thiophene-fused π-conjugated compounds have been widely studied as organic semiconducting materials and found to exhibit high semiconducting performances [5,13-16].

Furan-containing π-conjugated compounds have attracted less attention until recently [17-27]. The oxygen atom possesses a smaller van der Waals radius than a sulfur atom. Accordingly, furan-containing π-conjugated compounds should be expected to form a denser packing structure in the solid state, which is one of the main requirements for high semiconducting properties [28-31]. In 2007, Nakamura and co-workers reported the synthesis of furan-fused ladder-type π-conjugated compounds, benzo[1,2-*b*:4,5-*b'*]difurans (BDFs) **1** and their application to OLEDs as hole-transporting materials (Figure 1) [32]. They also synthesized a series of isomeric BDFs (benzo[1,2-*b*:5,4-*b'*]difurans and benzo[1,2-*b*:6,5-*b'*]difurans) and studied their

structure–property relationship [33,34]. Furthermore, naphtho-difurans with a fused-naphthalene between two furan rings have been developed as organic semiconductors for OFETs [19,20]. In particular, the naphtho[2,1-*b*:6,5-*b*']difuran derivative **2** has been reported to demonstrate an excellent OFET mobility of 3.6 cm$^2 \cdot$V$^{-1} \cdot$s^{-1} [19]. Previously, we have reported the synthesis of dibenzo[*d*,*d*']benzo[1,2-*b*:4,5-*b*']difurans (*anti*-DBBDFs), which is also a π-extended homologue of BDF [35]. The OFET devices with an *anti*-DBBDF skeleton exhibited p-type semiconducting properties [36,37]. For example, dialkyl-substituted *anti*-DBBDF **3** showed a hole mobility of 0.042 cm$^2 \cdot$V$^{-1} \cdot$s^{-1} [38]. Recently, we have also found that dinaphtho[2,3-*d*:2',3'-*d*']benzo[1,2-*b*:4,5-*b*']difuran (*anti*-DNBDF **4**) with a more extended π-conjugation afforded higher hole mobility of 0.33 cm$^2 \cdot$V$^{-1} \cdot$s^{-1} [39-41]. These studies clearly demonstrate that furan-fused π-conjugated compounds are promising candidates as organic semiconducting materials, and it is highly desirable to investigate the structure–property relationship thor-oughly for further development of furan-containing semiconducting materials.

Herein we report the synthesis of ladder-type π-conjugated compounds containing a benzo[2,1-*b*:3,4-*b*']difuran skeleton, such as dibenzo[*d*,*d*']benzo[2,1-*b*:3,4-*b*']difuran (*syn*-DBBDF **5**) and dinaphtho[2,3-*d*:2',3'-*d*']benzo[2,1-*b*:3,4-*b*']difuran (*syn*-DNBDF **6**, Figure 1) [42-46]. The physical and electrochemical properties of the synthesized compounds are also discussed. OFETs with these compounds as semiconducting layers were found to exhibit relatively high hole mobility of <1.0 × 10^{-1} cm$^2 \cdot$V$^{-1} \cdot$s^{-1}.

Results and Discussion
Synthesis
The synthetic routes to *syn*-DBBDF **5** and *syn*-DNBDF **6** are described in Scheme 1 and Scheme 2. 3-Decylanisole was first synthesized from commercially available 3-bromoanisole via
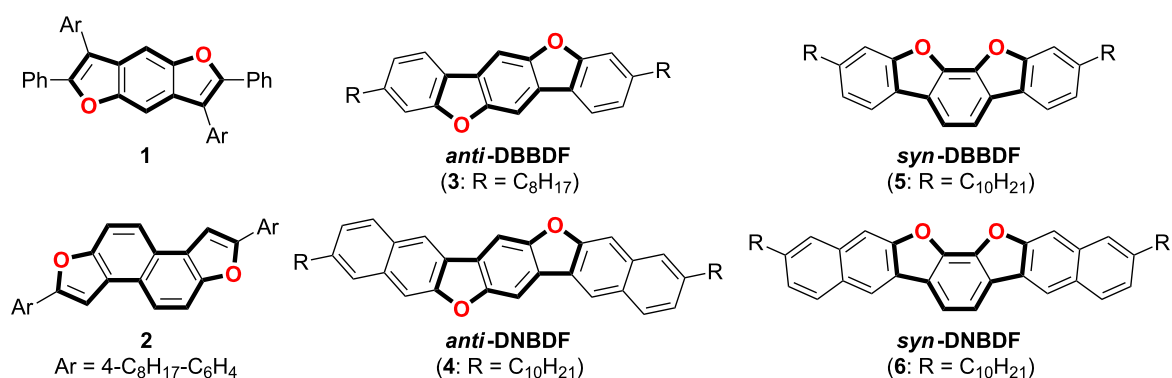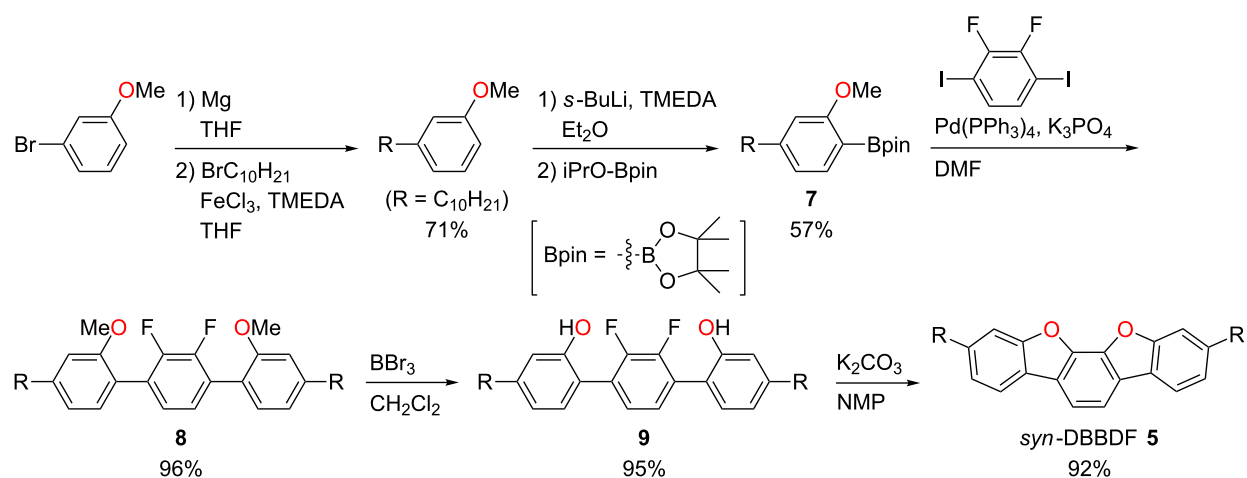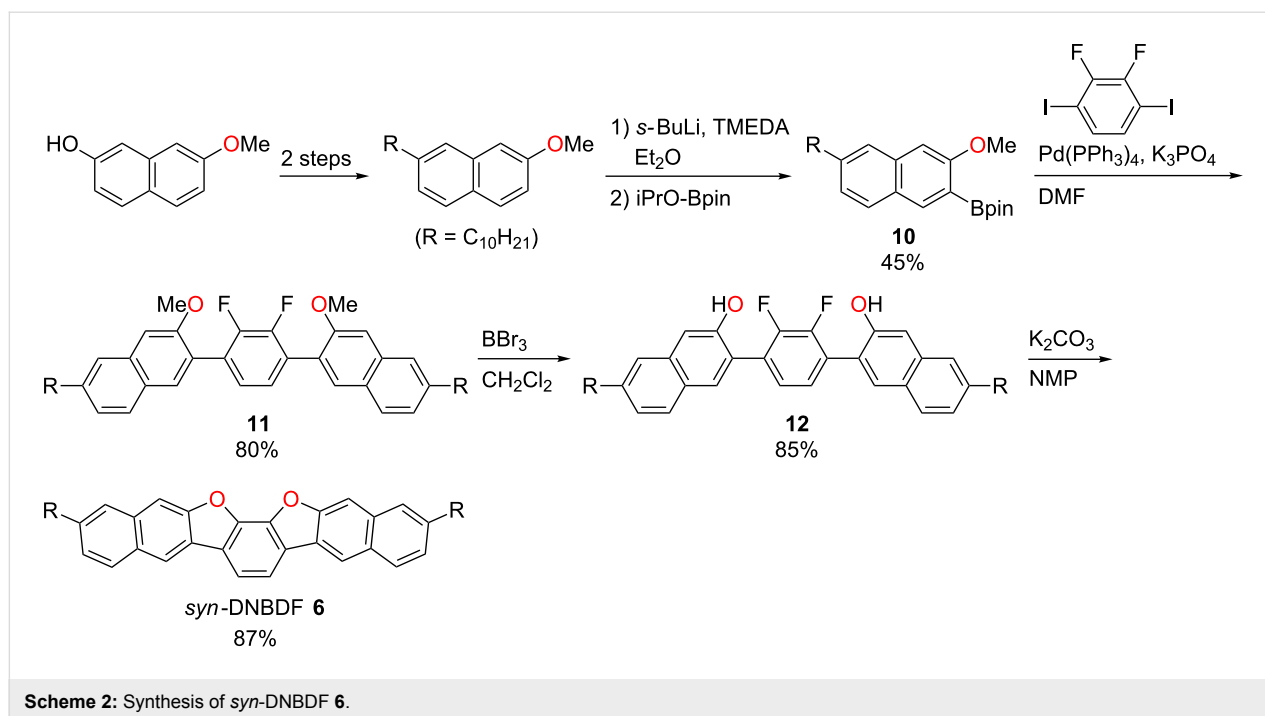

Figure 1: Structures of furan-fused ladder-type π-conjugated compounds.

Scheme 1: Synthesis of *syn*-DBBDF **5**.

Scheme 2: Synthesis of *syn*-DNBDF **6**.

iron-catalyzed cross-coupling reaction with decylmagnesium bromide in 71% yield [47]. Lithiation of the obtained 3-decyl-anisole with *s*-BuLi and the following treatment with 2-isopropoxy-4,4,5,5-tetramethyl-1,3,2-dioxaborolane (iPrO-Bpin) gave boronate ester **7** in 57% yield. Then, terphenyl **9** was synthesized via palladium-catalyzed Suzuki–Miyaura cross coupling of boronate ester **7** with 2,3-difluoro-1,4-diiodobenzene (96% yield) and subsequent demethylation (95% yield). Finally, the desired *syn*-DBBDF **5** was successfully synthesized via the double intramolecular cyclization under basic conditions at high temperature (92% yield) [37,43]. The same synthetic strategy was applied to the synthesis of *syn*-DNBDF (Scheme 2). 2-Decyl-7-methoxynaphthalene was prepared from 7-methoxynaphthalen-2-ol in two steps according to the literature [23,48], and used for the synthesis of boronate ester **10** (45% yield). The following cross coupling (80% yield), demethylation (85% yield), and the double cyclization (87% yield) gave the target *syn*-DNBDF **6**. The obtained *syn*-DBBDF **5** is soluble in common organic solvents and can be purified by column chromatography. In contrast, because of low solubility in common organic solvents, the crude product of *syn*-DNBDF **6** was purified by washing several times with water and the subsequent sublimation.

Thermal properties

The phase-transition properties and thermal stability of *syn*-DBBDF **5** and *syn*-DNBDF **6** were evaluated by differential scanning calorimetry (DSC) and thermogravimetric analysis (TGA), respectively. The DSC scans of *syn*-DBBDF **5** and

syn-DNBDF **6** showed some transition peaks with the first phase-transition temperature at 20 °C and 45 °C, respectively, in the heating process (Figure 2a). Such phase-transition temperatures are >50 °C lower than those of their *anti*-isomers **3**
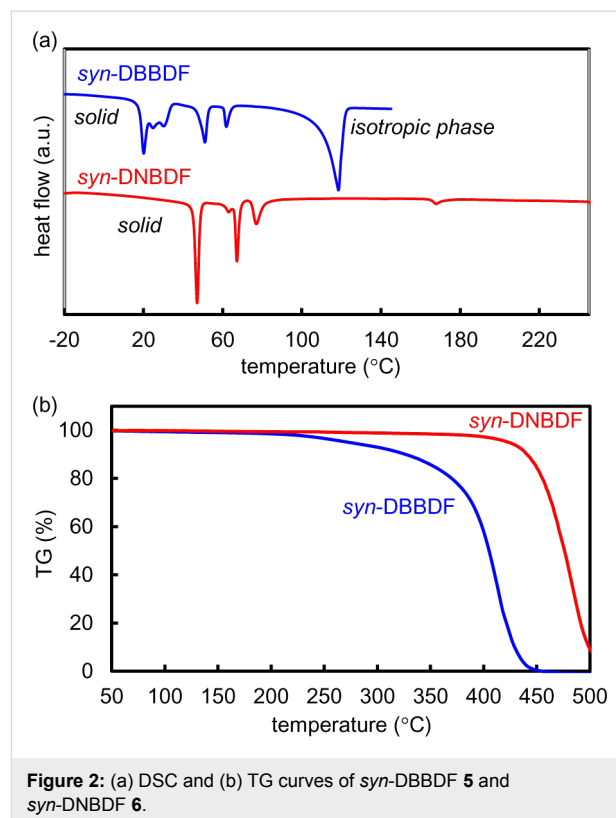

Figure 2: (a) DSC and (b) TG curves of *syn*-DBBDF **5** and *syn*-DNBDF **6**.

Table 1: Photophysical and electrochemical properties of *syn/anti*-DBBDFs and DNBDFs.

Compound	λ_{abs} (nm)[a]	λ_{em} (nm)[b]	Φ (%)[c]	Stokes shift (cm^{-1})	E_g (eV)[d]	$E_{ox}{}^{onset}$ (V)[e]	E_{HOMO} (eV)[f]
syn-DBBDF **5**	324	328	18	376	3.72	0.84	−5.64
syn-DNBDF **6**	365	370	61	370	3.32	0.56	−5.36
anti-DBBDF **3**	342	–	–	–	3.51	–	–
anti-DNBDF **4**	394	–	–	–	3.15	–	–

[a]In CHCl$_3$ (1.0 × 10^{-5} M). [b]In CHCl$_3$ (1.0 × 10^{-7} M). Excitation at 310 nm. [c]Absolute quantum yield determined by a calibrated integrating sphere system. Excitation at 275 nm for *syn*-DBBDF **5** and *syn*-DNBDF **6**. [d]Optical band gaps estimated from the onset position of the UV–vis absorption spectra in solution. [e]Onset potentials (vs Fc/Fc$^+$) of the first oxidation wave determined by cyclic voltammetry: 1.0 mM solution in CH$_2$Cl$_2$ (*syn*-DBBDF **5**) or Cl$_2$CHCHCl$_2$ (*syn*-DNBDF **6**) with 0.1 M Bu$_4$NClO$_4$, Pt as working and counter electrodes, scan rate = 50 mV·s^{-1}. [f]Calculated according to E_{HOMO} = −(E_{ox} + 4.80) eV (Fc/Fc$^+$ redox couple: 4.8 eV below the vacuum level).

and **4** [38,39]. These results indicate that *syn*-DBBDF **5** and *syn*-DNBDF **6** form weaker intermolecular interactions in the solid state than their corresponding *anti*-isomers. The mesophase of *syn*-DBBDF **5** was converted to the isotropic phase at 115 °C, while *syn*-DNBDF **6** did not melt below 250 °C. From the TG measurement, the temperatures of 5% weight loss (T_{d5}) of *syn*-DBBDF **5** and *syn*-DNBDF **6** were estimated to be 272 °C and 423 °C, respectively (Figure 2b).

Photophysical properties

The UV–vis spectrum of *syn*-DBBDF **5** in chloroform showed the strongest absorption maximum at 324 nm, while *syn*-DNBDF **6** showed a red-shifted absorption spectrum with the strongest absorption maximum at 365 nm (Figure 3a and Table 1). Since s*yn*-DNBDF **6** contains one more benzene ring at each terminal of the π-conjugated skeleton than *syn*-DBBDF **5**, it should possess an extended π-conjugation length, resulting in a red-shifted absorption spectrum. The HOMO–LUMO energy gaps estimated from the absorption edges were 3.72 eV and 3.32 eV for *syn*-DBBDF **5** and *syn*-DNBDF **6**, respectively. Their photoluminescence spectra as shown in Figure 3b exhibited mirror images of their absorption spectra with small Stokes shifts (376 cm^{-1} for *syn*-DBBDF **5**; 370 cm^{-1} for *syn*-DNBDF **6**), which reflect their high rigidity. Similar to its absorption spectra, *syn*-DNBDF **6** showed a red-shifted emission band with a relatively high quantum yield (Φ = 61% in CHCl$_3$ solution).

To investigate the structure–property relationship of DBBDFs and DNBDFs, the optical properties of *syn*-DBBDF **5** and *syn*-DNBDF **6** were compared with those of *anti*-DBBDF **3** and *anti*-DNBDF **4**. The UV–vis spectra of *anti*-DBBDF **3** and *anti*-DNBDF **4** were reported to show absorption maxima (342 nm for *anti*-DBBDF **3**; 394 nm for *anti*-DNBDF **4**) and absorption edges [353 nm (3.51 eV) for *anti*-DBBDF **3**; 410 nm (3.15 eV) for *anti*-DNBDF **4**] at longer wavelengths than *syn*-DBBDF **5** and *syn*-DNBDF **6**, respectively [38,39]. Accordingly, *syn*-isomers are indicated to possess shorter π-conjugation lengths than *anti*-isomers.
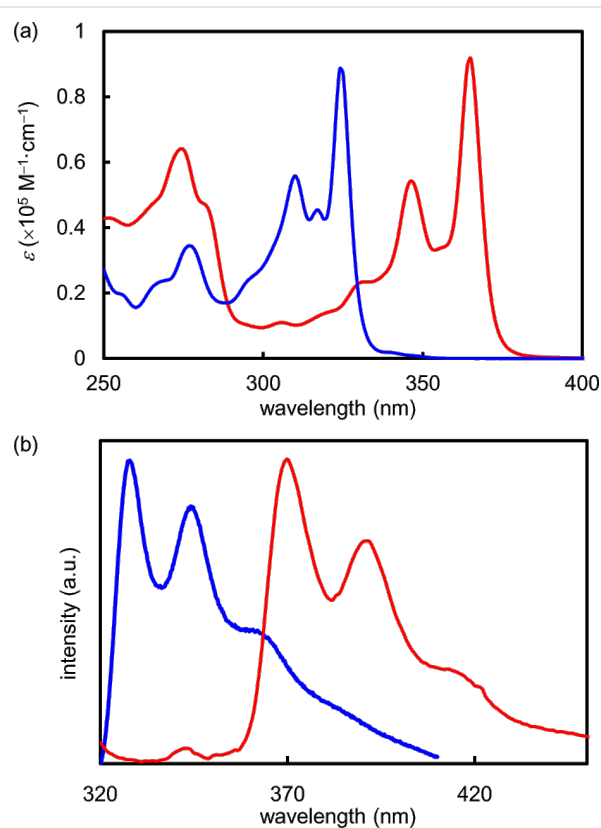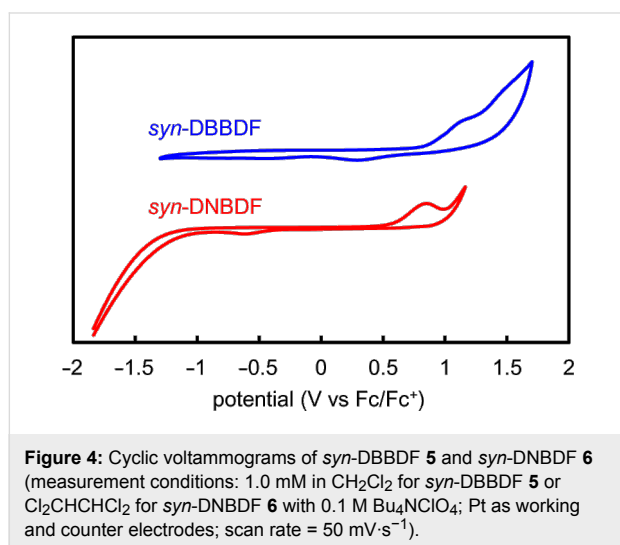

Figure 3: (a) UV–vis absorption spectra of *syn*-DBBDF **5** (blue line) and *syn*-DNBDF **6** (red line) in CHCl$_3$ (1.0 × 10^{-5} M) and (b) normalized photoluminescence spectra of *syn*-DBBDF **5** (blue line) and *syn*-DNBDF **6** (red line) in CHCl$_3$ (1.0 × 10^{-7} M).

Electrochemical properties

Cyclic voltammograms of *syn*-DBBDF **5** and *syn*-DNBDF **6** are shown in Figure 4 [1.0 mM solution in CH$_2$Cl$_2$ (*syn*-DBBDF **5**) or Cl$_2$CHCHCl$_2$ (*syn*-DNBDF **6**) with 0.10 M Bu$_4$NClO$_4$], and the electrochemical properties were summarized in Table 1. *syn*-DBBDF **5** exhibited two oxidation waves, and an onset potential of the first oxidation wave was determined to be 0.84 V (vs Fc/Fc$^+$). Accordingly, the HOMO energy level was estimated to be −5.64 eV under the premise that the energy

level of Fc/Fc$^+$ is 4.8 eV below the vacuum level [49-51]. In contrast, *syn*-DNBDF **6** showed one oxidation wave with an onset potential of 0.56 eV (vs Fc/Fc$^+$, HOMO = −5.36 eV). The lower oxidation potential and higher HOMO energy level of *syn*-DNBDF **6** should reflect its longer π-conjugation length than *syn*-DBBDF **5**. Based on their HOMO energy levels and HOMO−LUMO energy gaps, *syn*-DBBDF **5** and *syn*-DNBDF **6** are expected to work as stable semiconducting materials under ambient conditions.

Figure 4: Cyclic voltammograms of *syn*-DBBDF **5** and *syn*-DNBDF **6** (measurement conditions: 1.0 mM in CH$_2$Cl$_2$ for *syn*-DBBDF **5** or Cl$_2$CHCHCl$_2$ for *syn*-DNBDF **6** with 0.1 M Bu$_4$NClO$_4$; Pt as working and counter electrodes; scan rate = 50 mV·s^{-1}).

Fabrication of OFETs with *syn*-DBBDF- and *syn*-DNBDF-based thin films and evaluation of semiconducting properties

To study the semiconducting properties of *syn*-DBBDF **5** and *syn*-DNBDF **6**, bottom-gate/top-contact OTFTs were utilized as a device structure. Thin films of *syn*-DBBDF **5** and *syn*-DNBDF **6** were deposited by sublimation under high vacuum ($p < 10^{-5}$ Pa) at a rate of ca. 1 Å·s^{-1} for *syn*-DBBDF and ca. 0.4 Å·s^{-1} for *syn*-DNBDF onto the Si/SiO$_2$ substrates. The substrate temperature (T_{sub}) during deposition has been known to have a great impact on the OTFT performance by affecting the nucleation and growth of the organic molecules [52,53]. Accordingly, the thin films were fabricated at different substrate temperatures. In addition to the bare Si/SiO$_2$ substrates, the HMDS (hexamethyldisilazane)-treated substrates were used to evaluate the effect of the substrate structure on the device performance. The gold source/drain electrodes were deposited on the thin films. The channel width and length were 500 μm and 50 μm, respectively.

Both *syn*-DBBDF- and *syn*-DNBDF-based OFETs demonstrated typical p-type semiconducting characteristics. The extracted FET parameters and the transfer/output characteristics are summarized in Table 2, Figure 5, and Figure S21 (Supporting Information File 1). The *syn*-DBBDF-based OFETs fabricated on bare Si/SiO$_2$ substrates at T_{sub} = 30 °C showed a field-effect mobility μ$_{FET}$ of 5.0×10^{-5} cm^2·V^{-1}·s^{-1} and an I_{on}/I_{off} ratio of 10^1, while those with HMDS-treated substrates demonstrated higher mobility of 1.5×10^{-3} cm^2·V^{-1}·s^{-1} with an I_{on}/I_{off} ratio of 10^3. The deposition of *syn*-DBBDF **5** at T_{sub} = 60 °C did not give a thin film, which should be caused by re-sublimation of *syn*-DBBDF **5** from the surface. The more π-extended *syn*-DNBDF **6** afforded higher performances than *syn*-DBBDF **5**. OFETs fabricated on the bare and HMDS-treated Si/SiO$_2$ substrates at T_{sub} = 30 °C showed a field-effect mobility of 2.3×10^{-2} cm^2·V^{-1}·s^{-1} (I_{on}/I_{off} = 10^3) and 2.0×10^{-2} cm^2·V^{-1}·s^{-1} (I_{on}/I_{off} = 10^3), respectively. The FET performance also depends on the substrate temperature during thin-film fabrication. Thus, the highest hole mobility of 1.0×10^{-1} cm^2·V^{-1}·s^{-1} was obtained for the *syn*-DNBDF-based device fabricated on the HMDS-treated substrate at T_{sub} = 90 °C, while it was lower than that fabricated with *anti*-DNBDF derivatives [39].

Analysis of thin films

The vapor-deposited thin films of *syn*-DBBDF **5** and *syn*-DNBDF **6** were analyzed by X-ray diffraction (XRD) and atomic force microscopy (AFM). Figure 6 shows the out-of-plane XRD pattern and an AFM image of the thin film of *syn*-DNBDF **6** on the HMDS-treated Si/SiO$_2$ substrate (T_{sub} = 90 °C), which demonstrated the highest mobility in this study. The layer structure was confirmed with a monolayer thickness (*d*-spacing) of 3.94 nm (2θ = 2.24°). Molecular lengths with ex-

Table 2: FET characteristics.

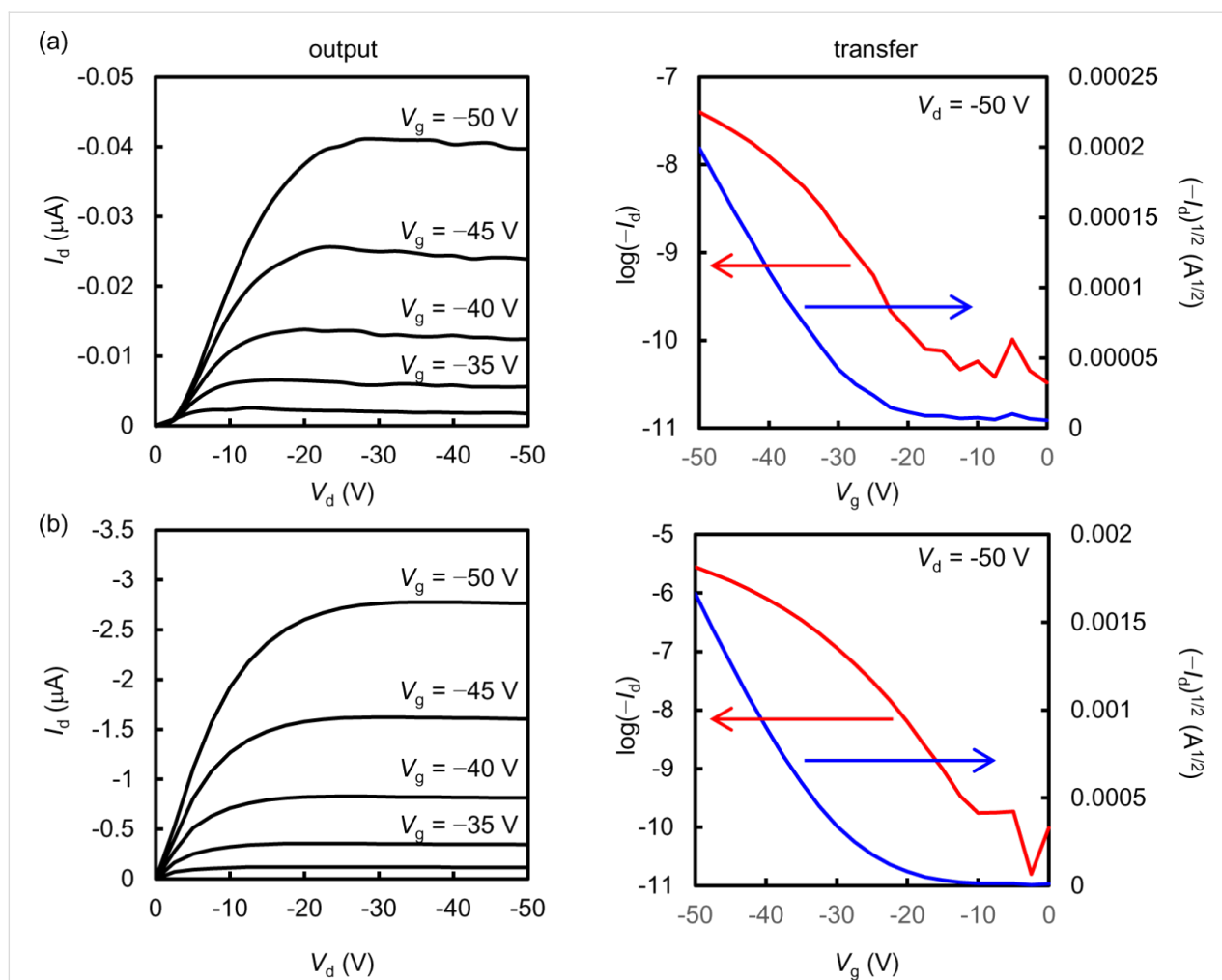| Compound	Surfactant	T_{sub} (°C)	μ$_{FET}$ (cm^2·V^{-1}·s^{-1})	V_{th} (V)	I_{on}/I_{off}
syn-DBBDF **5**	–	30	5.0×10^{-5}	−26	10^1
	HMDS	30	1.5×10^{-3}	−25	10^3
syn-DNBDF **6**	–	30	2.3×10^{-2}	−24	10^3
	–	90	6.5×10^{-2}	−25	10^4
	HMDS	30	2.0×10^{-2}	−22	10^3
	HMDS	90	1.0×10^{-1}	−28	10^5

Figure 5: Output and transfer characteristics of the representative OFETs with a thin film of (a) *syn*-DBBDF **5** (T_{sub} = 30 °C) and (b) *syn*-DNBDF **6** (T_{sub} = 90 °C) on HMDS-treated Si/SiO$_2$ substrates.

tended linear alkyl chains are expected to be ca. 4.2 nm. Accordingly, *syn*-DNBDF **6** should be arranged on the substrate with its molecular long axis almost perpendicular to the sub-

strate. Such a layer structure was also confirmed by AFM. As shown in Figure 6b,c, the thin film of *syn*-DNBDF **6** forms relatively large grains (ca. 0.5 μm in size) with a layer structure
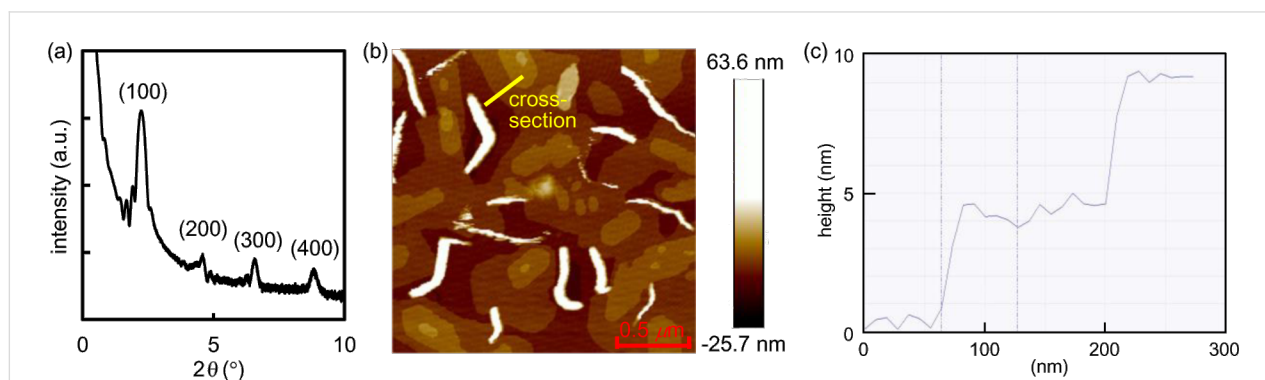

Figure 6: (a) XRD pattern, (b) AFM image (2 × 2 μm), and (c) cross-section height of a thin film of *syn*-DNBDF **6** on HMDS-treated Si/SiO$_2$ substrates (T_{sub} = 90 °C).

(step heights ca. 4.0 nm) along with heterogeneous protrusions. The molecular arrangement indicated by these observations is advantageous for the in-plane charge transfer of OFETs. Based on XRD patterns and AFM images, the substrate treatment and the substrate temperature seem to have a limited impact on the molecular arrangement (Figures S22 and S23, Supporting Information File 1). The similar layer structure was also confirmed for *syn*-DBBDF **5** (Figures S22 and S23, Supporting Information File 1).

Conclusion

In summary, we investigated the synthesis and properties of ladder-type π-conjugated compounds, dibenzo[*d,d'*]benzo[2,1-*b*:3,4-*b'*]difuran (*syn*-DBBDF **5**) and dinaphtho[2,3-*d*:2',3'-*d'*]benzo[2,1-*b*:3,4-*b'*]difuran (*syn*-DNBDF **6**). Based on the photophysical and electrochemical data, both compounds are expected to possess good air stability as organic semiconducting materials. The comparison with their *anti*-isomers revealed that the π-conjugation in *syn*-DBBDF **5** and *syn*-DNBDF **6** is less effective than those of their *anti*-isomers. OFETs based on these compounds were fabricated as bottom-gate top-contact devices, and their semiconducting properties were evaluated. All devices showed typical p-type transistor characteristics. The highest hole mobility of 1.0×10^{-1} cm$^2 \cdot$V$^{-1} \cdot$s^{-1} was achieved when using *syn*-DNBDF-based OFET device.

Supporting Information

Supporting Information File 1

General experimental procedures, synthetic procedures/characterization data of compounds **5**–**12**, device fabrication/evaluation procedures, OFET characteristics, XRD patterns, and AFM images.
[http://www.beilstein-journals.org/bjoc/content/supplementary/1860-5397-12-79-S1.pdf]

Acknowledgements

References

1. Anthony, J. E. *Chem. Rev.* **2006,** *106,* 5028–5048. doi:10.1021/cr050966z
2. Bao, Z.; Locklin, J. *Organic Field-Effect Transistors;* CRC Press: Boca Raton, 2007. doi:10.1201/9781420008012
3. Murphy, A. R.; Fréchet, J. M. J. *Chem. Rev.* **2007,** *107,* 1066–1096. doi:10.1021/cr0501386
4. Allard, S.; Forster, M.; Souharce, B.; Thiem, H.; Scherf, U. *Angew. Chem., Int. Ed.* **2008,** *47,* 4070–4098. doi:10.1002/anie.200701920
5. Takimiya, K.; Shinamura, S.; Osaka, I.; Miyazaki, E. *Adv. Mater.* **2011,** *23,* 4347–4370. doi:10.1002/adma.201102007
6. Wang, C.; Dong, H.; Hu, W.; Liu, Y.; Zhu, D. *Chem. Rev.* **2012,** *112,* 2208–2267. doi:10.1021/cr100380z
7. Mei, J.; Diao, Y.; Appleton, A. L.; Fang, L.; Bao, Z. *J. Am. Chem. Soc.* **2013,** *135,* 6724–6746. doi:10.1021/ja400881n
8. Kraft, A.; Grimsdale, A. C.; Holmes, A. B. *Angew. Chem., Int. Ed.* **1998,** *37,* 402–428. doi:10.1002/(SICI)1521-3773(19980302)37:4<402::AID-ANIE402>3.0. CO;2-9
9. Kafafi, Z. *Organic Electroluminescence;* CRC Press: Boca Raton, 2005. doi:10.1201/9781420028201
10. Müllen, K.; Scherf, U. *Organic Light-Emitting Devices: Synthesis, Properties and Applications;* Wiley-VCH Verlag GmbH & Co. KGaA: Weinheim, 2006. doi:10.1002/3527607986.fmatter
11. Sun, S.-S.; Sariciftci, N. S. *Organic Photovoltaics: Mechanism, Materials, and Devices;* CRC Press: Boca Raton, 2005.
12. Scharber, M. C.; Mühlbacher, D.; Koppe, M.; Denk, P.; Waldauf, C.; Heeger, A. J.; Brabec, C. J. *Adv. Mater.* **2006,** *18,* 789–794. doi:10.1002/adma.200501717
13. Perepichka, I. F.; Perepichka, D. F. *Handbook of Thiophene-Based Materials: Applications in Organic Electronics and Photonics;* John Wiley & Sons Ltd.: Chichester, U.K., 2009. doi:10.1002/9780470745533
14. Wu, W.; Liu, Y.; Zhu, D. *Chem. Soc. Rev.* **2010,** *39,* 1489–1502. doi:10.1039/B813123F
15. Youn, J.; Kewalramani, S.; Emery, J. D.; Shi, Y.; Zhang, S.; Chang, H. C.; Liang, Y. J.; Yeh, C. M.; Feng, C. Y.; Huang, H.; Stern, C.; Chen, L. H.; Ho, J. C.; Chen, M. C.; Bedzyk, M. J.; Facchetti, A.; Marks, T. J. *Adv. Funct. Mater.* **2013,** *23,* 3850–3865. doi:10.1002/adfm.201203439
16. Cinar, M. E.; Ozturk, T. *Chem. Rev.* **2015,** *115,* 3036–3140. doi:10.1021/cr500271a
17. Li, H.; Jiang, P.; Yi, C.; Li, C.; Liu, S.-X.; Tan, S.; Zhao, B.; Braun, J.; Meier, W.; Wandlowski, T.; Decurtins, S. *Macromolecules* **2010,** *43,* 8058–8062. doi:10.1021/ma101693d
18. Kobilka, B. M.; Dubrovskiy, A. V.; Ewan, M. D.; Tomlinson, A. L.; Larock, R. C.; Chaudhary, S.; Jeffries-El, M. *Chem. Commun.* **2012,** *48,* 8919–8921. doi:10.1039/c2cc34070d
19. Mitsui, C.; Soeda, J.; Miwa, K.; Tsuji, H.; Takeya, J.; Nakamura, E. *J. Am. Chem. Soc.* **2012,** *134,* 5448–5451. doi:10.1021/ja2120635
20. Nakano, M.; Mori, H.; Shinamura, S.; Takimiya, K. *Chem. Mater.* **2012,** *24,* 190–198. doi:10.1021/cm202853b
21. Watanabe, M.; Su, W.-T.; Chang, Y. J.; Chao, T.-H.; Wen, Y.-S.; Chow, T. J. *Chem. – Asian J.* **2013,** *8,* 60–64. doi:10.1002/asia.201200834
22. Mitsui, C.; Okamoto, T.; Matsui, H.; Yamagishi, M.; Matsushita, T.; Soeda, J.; Miwa, K.; Sato, H.; Yamano, A.; Uemura, T.; Takeya, J. *Chem. Mater.* **2013,** *25,* 3952–3956. doi:10.1021/cm303376g
23. Nakahara, K.; Mitsui, C.; Okamoto, T.; Yamagishi, M.; Matsui, H.; Ueno, T.; Tanaka, Y.; Yano, M.; Matsushita, T.; Soeda, J.; Hirose, Y.; Sato, H.; Yamano, A.; Takeya, J. *Chem. Commun.* **2014,** *50,* 5342–5344. doi:10.1039/C3CC47577H

24. Shi, S.; Xie, X.; Gao, C.; Shi, K.; Chen, S.; Yu, G.; Guo, L.; Li, X.; Wang, H. *Macromolecules* **2014,** *47,* 616–625. doi:10.1021/ma402107n
25. Moussalem, C.; Segut, O.; Gohier, F.; Allain, M.; Frère, P. *ACS Sustainable Chem. Eng.* **2014,** *2,* 1043–1048. doi:10.1021/sc500042u
26. Du, Z.; Chen, Y.; Chen, W.; Qiao, S.; Wen, S.; Liu, Q.; Zhu, D.; Sun, M.; Yang, R. *Chem. – Asian J.* **2014,** *9,* 2621–2627. doi:10.1002/asia.201402467
27. Mitsui, C.; Soeda, J.; Miwa, K.; Shoyama, K.; Ota, Y.; Tsuji, H.; Takeya, J.; Nakamura, E. *Bull. Chem. Soc. Jpn.* **2015,** *88,* 776–783. doi:10.1246/bcsj.20150033
28. Hutchison, G. R.; Ratner, M. A.; Marks, T. J. *J. Am. Chem. Soc.* **2005,** *127,* 16866–16881. doi:10.1021/ja0533996
29. Gidron, O.; Diskin-Posner, Y.; Bendikov, M. *J. Am. Chem. Soc.* **2010,** *132,* 2148–2150. doi:10.1021/ja9093346
30. Huang, J.-D.; Wen, S.-H.; Deng, W.-Q.; Han, K.-L. *J. Phys. Chem. B* **2011,** *115,* 2140–2147. doi:10.1021/jp108125q
31. Gidron, O.; Dadvand, A.; Sheynin, Y.; Bendikov, M.; Perepichka, D. F. *Chem. Commun.* **2011,** *47,* 1976–1978. doi:10.1039/C0CC04699J
32. Tsuji, H.; Mitsui, C.; Ilies, L.; Sato, Y.; Nakamura, E. *J. Am. Chem. Soc.* **2007,** *129,* 11902–11903. doi:10.1021/ja074365w
33. Tsuji, H.; Mitsui, C.; Sato, Y.; Nakamura, E. *Heteroat. Chem.* **2011,** *22,* 316–324. doi:10.1002/hc.20682
34. Mitsui, C.; Tanaka, H.; Tsuji, H.; Nakamura, E. *Chem. – Asian J.* **2011,** *6,* 2296–2300. doi:10.1002/asia.201100326
35. Kawaguchi, K.; Nakano, K.; Nozaki, K. *J. Org. Chem.* **2007,** *72,* 5119–5128. doi:10.1021/jo070427p
36. Kawaguchi, K. Synthesis of Heteroacenes and Their Applications to Organic Functional Materials. Ph.D. Thesis, The University of Tokyo, Tokyo, 2008.
37. Kitamura, T.; Takaku, K.; Sotoyama, W. Organic thin film transistor having benzobisbenzofuran derivative-containing semiconductor active layer, organic semiconductor thin film, and organic semiconductor material. JP 2014045099, March 13, 2014.
38. Nakano, K.; Chayama, N.; Truong, M. A.; Kawaguchi, K.; Nozaki, K. *Polym. Prepr., Jpn.* **2011,** *60,* 4144–4145.
39. Yamagata, Y.; Nakano, K. Abstracts of Papers. The 94th annual Meeting of The Chemical Society of Japan, Nagoya, March 27–30, 2014; The Chemical Society of Japan: Tokyo, 2014; 4A7-35.
40. Okamoto, T.; Mitsui, C.; Yamagishi, M.; Nakamura, K.-I.; Nakahara, K.; Soeda, J.; Hirose, Y.; Sato, H.; Yamano, A.; Takeya, J. Abstracts of Papers. The 61st JSAP Spring Meeting, Sagamihara, March 17–20, 2014; The Japan Society of Applied Physics, 2014; pp 12–260.
41. Takeya, J.; Okamoto, T.; Mitsui, C.; Matsushita, T. Preparation of chalcogen-containing organic compounds as semiconductor materials. WO 2014136827, Sept 12, 2014.
42. Solution-processed OFETs with *syn*-DBBDFs and *syn*-DNBDFs have been reported in the patent. However, the detailed description was not given for their synthesis, characterization, and physical properties. See reference [43].
43. Kitamura, T.; Takaku, K.; Toyama, W. Organic thin-film transistor, benzobisbenzofuran compound, coating solution for non-emitting organic semiconductor device, organic semiconductor thin film, and organic semiconductor material. JP 2014082248, May 8, 2014.
44. For π-conjugated molecules with a *syn*-DBBDF or *syn*-DNBDF skeleton, see references [45,46].
45. Nakanishi, K.; Sasamori, T.; Kuramochi, K.; Tokitoh, N.; Kawabata, T.; Tsubaki, K. *J. Org. Chem.* **2014,** *79,* 2625–2631. doi:10.1021/jo500085a
46. Nakanishi, K.; Fukatsu, D.; Takaishi, K.; Tsuji, T.; Uenaka, K.; Kuramochi, K.; Kawabata, T.; Tsubaki, K. *J. Am. Chem. Soc.* **2014,** *136,* 7101–7109. doi:10.1021/ja502209w
47. Nakamura, M.; Matsuo, K.; Ito, S.; Nakamura, E. *J. Am. Chem. Soc.* **2004,** *126,* 3686–3687. doi:10.1021/ja049744t
48. Mewshaw, R. E.; Edsall, R. J.; Yang, C.; Manas, E. S.; Xu, Z. B.; Henderson, R. A.; Keith, J. C., Jr.; Harris, H. A. *J. Med. Chem.* **2005,** *48,* 3953–3979. doi:10.1021/jm058173s
49. Pommerehne, J.; Vestweber, H.; Guss, W.; Mahrt, R. F.; Bassler, H.; Porsch, M.; Daub, J. *Adv. Mater.* **1995,** *7,* 551–554. doi:10.1002/adma.19950070608
50. Johansson, T.; Mammo, W.; Svensson, M.; Andersson, M. R.; Inganäs, O. *J. Mater. Chem.* **2003,** *13,* 1316–1323. doi:10.1039/B301403G
51. Cardona, C. M.; Li, W.; Kaifer, A. E.; Stockdale, D.; Bazan, G. C. *Adv. Mater.* **2011,** *23,* 2367–2371. doi:10.1002/adma.201004554
52. Kymissis, I. *Organic Field Effect Transistors: Theory, Fabrication and Characterization;* Springer Science+Business Media, LLC: New York, 2009.
53. Ling, M. M.; Bao, Z. *Chem. Mater.* **2004,** *16,* 4824–4840. doi:10.1021/cm0496117